GA–A23217

THE 110 GHz GYROTRON SYSTEM ON DIII–D: GYROTRON TESTS AND PHYSICS RESULTS

by

J. LOHR, P. CAHALAN, R.W. CALLIS, T.S. CHU,
J.S. deGRASSIE, I. GORELOV, H. IKEZI, R.A. LEGG,
T.C. LUCE, C.C. PETTY, D. PONCE, R. PRATER,
D.I. SCHUSTER, and S.E. TSIMRING

GENERAL ATOMICS PROJECT 30033
DECEMBER 1999

GA–A23217

THE 110 GHz GYROTRON SYSTEM ON DIII–D: GYROTRON TESTS AND PHYSICS RESULTS

by

J. LOHR, P. CAHALAN,[1] R.W. CALLIS, T.S. CHU,[1]
J.S. deGRASSIE, I. GORELOV, H. IKEZI, R.A. LEGG,
T.C. LUCE, C.C. PETTY, D. PONCE, R. PRATER,
D.I. SCHUSTER,[2] and S.E. TSIMRING

This is a preprint of a paper presented at the Fourth International Workshop on Strong Microwaves in Plasmas, August 2–9, 1999, Nizhny Novgorod, Russia, and to be printed in the *Proceedings.*

Work supported by
U.S. Department of Energy under
Contract DE-AC03-99ER54463

[1]Communications and Power Industries
[2]Brown University

GENERAL ATOMICS PROJECT 30033
DECEMBER 1999

THE 110 GHz GYROTRON SYSTEM ON DIII-D: GYROTRON TESTS AND PHYSICS RESULTS

J. Lohr, P. Cahalan, R.W. Callis, T.S. Chu,* J.S. deGrassie, I. Gorelov, H. Ikezi, R.A. Legg, T.C. Luce, C.C. Petty, D. Ponce, R. Prater, D.I. Schuster,† S.E. Tsimring,*

General Atomics, P.O. Box 85608, San Diego, California, 92186-5608, USA
*Communications and Power Industries, Palo Alto, California, U.S.A.
†Brown University, Providence, Rhode Island, U.S.A.

The DIII–D tokamak has installed a system with three gyrotrons at the 1 MW level operating at 110 GHz. Physics experiments on electron cyclotron current drive, heating, and transport have been performed. Good efficiency has been achieved both for on-axis and off-axis current drive with relevance for control of the current density profile leading to advanced regimes of tokamak operation, although there is a difference between off-axis ECCD efficiency inside and outside the magnetic axis. Heating efficiency is excellent and electron temperatures up to 10 keV have been achieved. The gyrotron system is versatile, with poloidal scan and control of the polarization of the injected rf beam. Phase correcting mirrors form a Gaussian beam and focus it into the waveguide. Both perpendicular and oblique launch into the tokamak have been used. Three different gyrotron designs are installed and therefore unique problems specific to each have been encountered, including parasitic oscillations, mode hops during modulation and polarization control problems. Two of the gyrotrons suffered damage during operations, one due to filament failure and one due to a vacuum leak. The repairs and subsequent testing will be described. The transmission system uses evacuated, windowless waveguide and the three gyrotrons have output windows of three different materials. One gyrotron uses a diamond window and generates a Gaussian beam directly. The development of the system and specific tests and results from each of the gyrotrons will be presented. The DIII–D project has committed to an upgrade of the system, which will add three gyrotrons in the 1 MW class, all using diamond output windows, to permit operation at up to ten seconds per pulse at one megawatt output for each gyrotron.

I. Introduction

The 110 GHz ECH system on the DIII-D tokamak comprises three different gyrotrons in the 1 MW class, one Gycom gyrotron and two CPI gyrotrons. The gyrotrons are of two general types, characterized by either a diode or triode magnetron injection gun (MIG) and are further differentiated by the power handling capability of their output windows, which in turn determines the designed characteristics of the output rf beams.

The characteristics and representative gyrotron typical best performance are summarized in Table 1.

Table 1. Gyrotron Characteristics

Manufac-turer	Gun type	Window	Performance	rf beam	Mfg. Type	Local name
Gycom[1]	diode MIG	BN	0.8 MW 2.0 s	broad	Centaur	Katya
CPI[2]	triode MIG	sapphire	1.1 MW 0.6 s	broad	8011A	Dorothy
CPS[3]	triode MIG	diamond	0.5 MW 4.2 s	Gaussian	8110	Toto

Measurements of the rf output power are made using calorimetry on the window cooling circuits. The BN window on Katya is edge cooled by water and has 3.7% absorption. The sapphire window on Dorothy is a face cooled double disk with a chloro-flurocarbon, FC-75, as the coolant. This window has 1.7% absorption. The window on Toto is a single diamond disk. For this window the absorption, approximately 0.33%, is too low for reliable calorimetric measurements, so output power was measured directly using a black planar load with 1,octanol as the working fluid. Octanol has linear absorption of 13 dB per cm traversed[4] and the load has minimum thickness of 2.6 cm. The output powers and rf generation efficiencies for each of the gyrotrons are presented in Fig. 1 (a,b,c).

The diode gyrotron has demonstrated somewhat better efficiency than either of the triode tubes. The triode tube produced the highest output power, 1.09 MW averaged over a 600 msec pulse, but the triode tube with the diamond output window has consistently had the worst rf efficiency, averaging 20%–25% in measurements at DIII–D. In initial tests of this gyrotron at CPI, a higher efficiency, about 30% was measured. The reason for the discrepancy is under investigation.

The internal optics systems in the gyrotrons are used to optimize the rf beams for use with the different windows. For the BN and sapphire windows, it was necessary to spread the Gaussian beams naturally produced by the internal mode converters so that the limiting power density was not exceeded on the window. For the Toto gyrotron, with its diamond window, the Gaussian beam could pass without exceeding the limiting power density, so in this gyrotron the Gaussian beam profile was maintained. The waveguide transmission lines used at DIII–D are corrugated circular aluminum tubes propagating the $HE_{1,1}$ circular waveguide

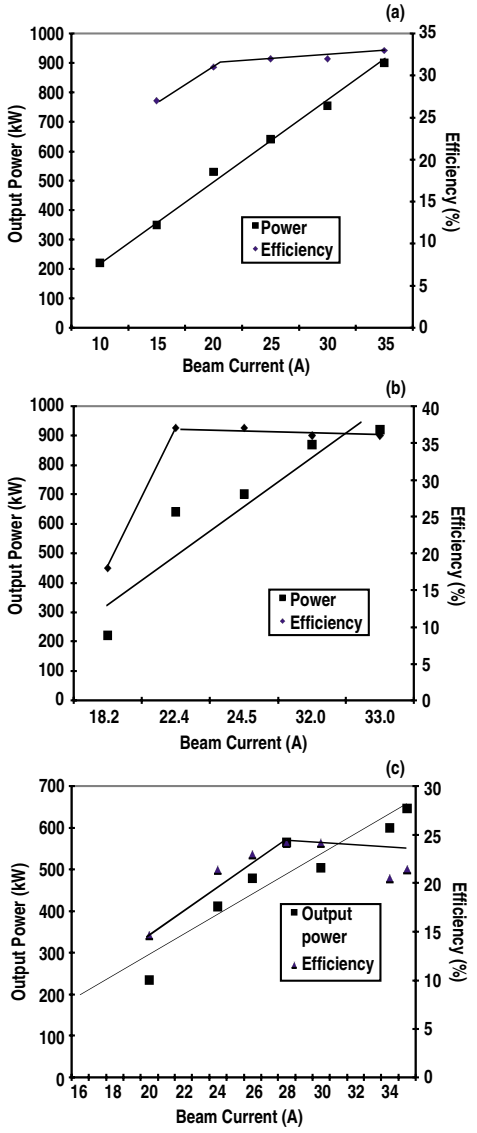

Fig. 1. The rf production efficiencies and output powers for the three gyrotrons, Katya, Dorothy, and Toto are shown in (a), (b), and (c) respectively. The highest output power, 1.09 MW averaged over a 600 msec pulse, was achieved by the triode gyrotron Dorothy, while the highest rf production efficiency was consistently achieved by the diode gyrotron Katya.

mode, which couples well to a Gaussian beam. Therefore the rf beams from Katya and Dorothy had to be restored to Gaussians by reflection from phase correcting mirrors and all three beams had to have Gaussian waists at the waveguide inputs with diameters of 20.3 mm, which is 64% of the diameter of the waveguide. Infrared camera views of the rf beam cross sections for the three gyrotrons near the output windows are shown in Fig. 2 (a,b,c), where this design requirement is clear.

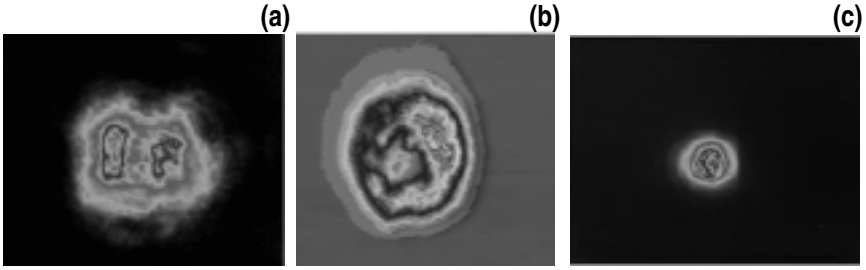

Fig. 2. Infrared camera pictures of the power profiles near the output windows for the three gyrotrons, Katya, Dorothy, and Toto are presented in (a), (b), and (c), respectively. The Toto gyrotron has a diamond output window and the internal optics are designed to produce a Gaussian output beam with a waist near the 5 cm diameter output window, but the other two gyrotrons, Katya and Dorothy, have windows with limiting power density capabilities, therefore the internal optics systems for these tubes spread the output rf beams over a large fraction of the 10 cm diameter windows.

The rf beams propagate into free space, and power profile measurements at several axial positions can be used to calculate the surfaces of phase correcting mirrors which can be used to reform Gaussian beams. This phase reconstruction technique[5–8] has been applied to the DIII–D systems and the resulting beams at the waveguide inputs are seen in Fig. 3 (a,b,c), produced using thermally sensitive paper at the waveguide inputs, to be well suited for exciting the $HE_{1,1}$ mode.

II. System Performance and Diagnostics

The gyrotron systems installed on DIII-D collectively have demonstrated all the requirements for advanced tokamak research at fusion parameters: Unit power $\geq$ 1 MW; Pulse lengths $\geq$ 2.0 sec; Gaussian beams; Low loss transmission over lines approaching 100 m in length; Control of the trajectory and polarization of the launched rf beam; and Excellent reliability. Repairable failures were experienced in the two

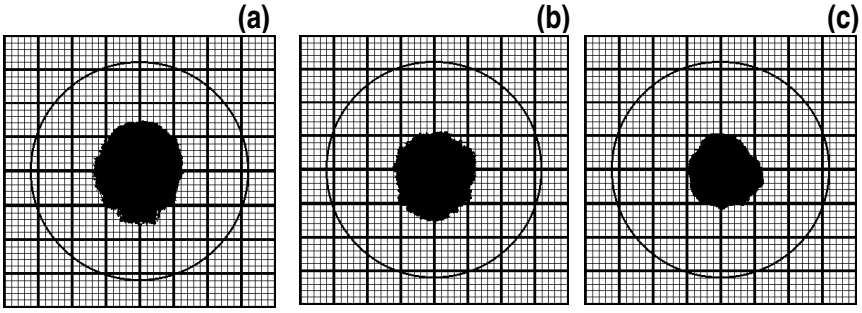

Fig. 3. The same rf beams shown in Fig 2 are shown in Fig. 3(a), (b), and (c) following reflection from pairs of mirrors especially designed to place a Gaussian waist with $w/a = 0.64$ at the input to the corrugated waveguides. The mirrors both focus and phase correct the beams produced by the gyrotrons. Thermally sensitive plotter paper is used to indicate the power profiles. The waveguide diameter, indicated by the circles, is 31.75 mm.

triode development gyrotrons. On Dorothy, which had about 5,000 hours of filament operation, the filament shorted, possibly due to an incorrect startup command sent by the control system. On Toto, there was a small failure in a braze in the collector region, which partially vented the gyrotron following a normal pulse. Toto has been repaired and is in test at CPI using its original gun, and Dorothy is ready to be reassembled following its repair. In each case, the cost of the repair was about 10% of the value of the gyrotron.

Polarization of the rf beam

The second harmonic extraordinary mode plasma wave is excited by the microwave beam in the DIII–D installation. In order to generate this mode using microwave injection at arbitrary toroidal and poloidal angles to the tokamak flux surfaces, it must be possible arbitrarily to control the elliptical polarization of the injected rf beam.[9] This is accomplished at DIII–D by use of grooved mirrors in two of the miter bends of the transmission line. The mirrors have sinusoidal grooves and rotate under remote control.

Measurement of the power deposition profile using Fourier analysis of $T_e(r,t)$ measured by the 32 channel heterodyne radiometer for modulated rf injection has been used to determine the actual injected polarization. The plasma wave excited by the rf can be viewed in the general case as a

superposition of extraordinary and ordinary mode waves. These two waves have substantially different power deposition profiles and wave refracion. The differences are particularly pronounced for off-axis injection.[10] In Fig. 4, the vacuum, X–mode, and O–mode trajectories are plotted, projected to the poloidal plane at the injector, for an rf beam injected with a 19° toroidal angle for current drive and a poloidal angle such that the wave encounters the plasma second harmonic resonance above the magnetic axis but near the major radius, R_0. For perfect X–mode, the optical depth is large enough that the absorption is essentially 100% in a single pass. For O–mode, the off-axis optical depth is small, first pass absorption is negligible and second pass absorption, where the wave trajectory crosses the resonance for the second time at a location with higher T_e, is only marginally greater. Although it was intended that the X–mode only be excited, the measured power deposition profile clearly reveals an O-mode component. These measurements indicated that determination of the injected polarization at the tokamak would be required fully to qualify the system.

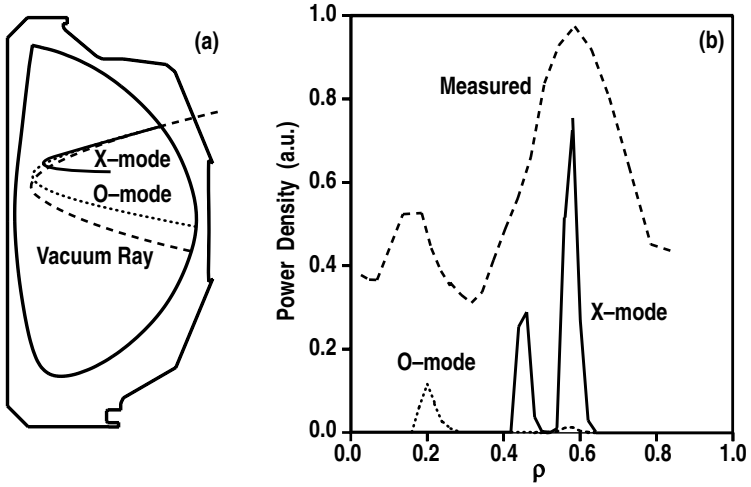

Fig. 4. The injected X–mode, O–mode, and the vacuum rf beam trajectories are shown projected to the poloidal plane of injection for a toroidal injection 19° off-perpendicular for current drive. The plasma second harmonic electron resonance is approximately on a vertical line at the major radius. The measured absorption profile has a peak associated with O–mode, although pure X–mode was intended to have been launched.

Measurements were made of the polarization of the rf beam using a polarimeter developed especially for the purpose.[11] Because of transient

behavior during the first few 100 msec of the gyrotron pulse, it was required that the polarimeter operate in vacuum at the full rf beam power, up to 1 MW, and for pulse lengths ≤ 300 msec.

The electric field vector of an electromagnetic wave in the general case traces out an ellipse in an $x-y$ plane perpendicular to its direction of propagation as indicated in Fig. 5. The wave polarization can be completely specified using the lengths of the elliptical axes a, b and the tilt angle α of one of the axes with respect to the laboratory reference. The special cases $b/a = -1,0,+1$ are called, respectively, left circular, linear and right circular polarization and for $b/a = 0$, $\alpha = 90^\circ$ and rf injection perpendicular to the flux surfaces, the X–mode will be excited in the plasma.

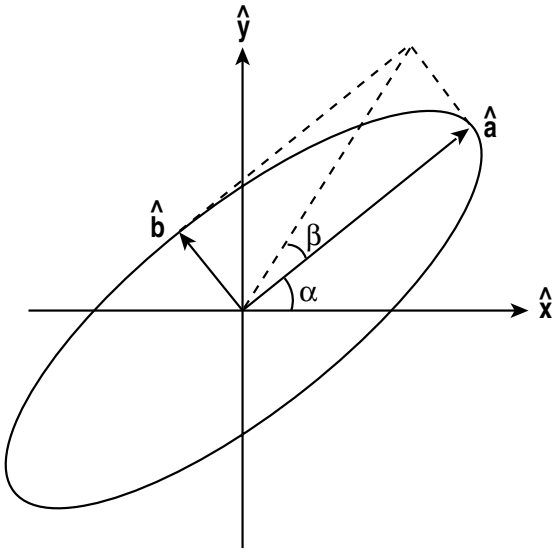

Fig. 5. Coordinate system for describing arbitrary elliptical polarization of the rf beam. The cases $b/a = -1$, 0, +1 are, respectively, left hand, linear, and right hand circular polarization. Parameters $\alpha = 90^\circ$, $b/a = 0$ would be used to excite X–mode for injection perpendicular to the magnetic field.

The analyzer samples the waveguide rf beam using a d iamond pickoff mirror mounted in a miter bend with about –40 dB coupling coefficient. The polarimeter consists of a rotating birefringent quarter wave plate and a fundamental waveguide detection system. The analyzer is shown schematically in Fig. 6. For an 800 kW microwave beam and 300 msec pulse length, the pickoff mirror peak temperature was 150˚C without

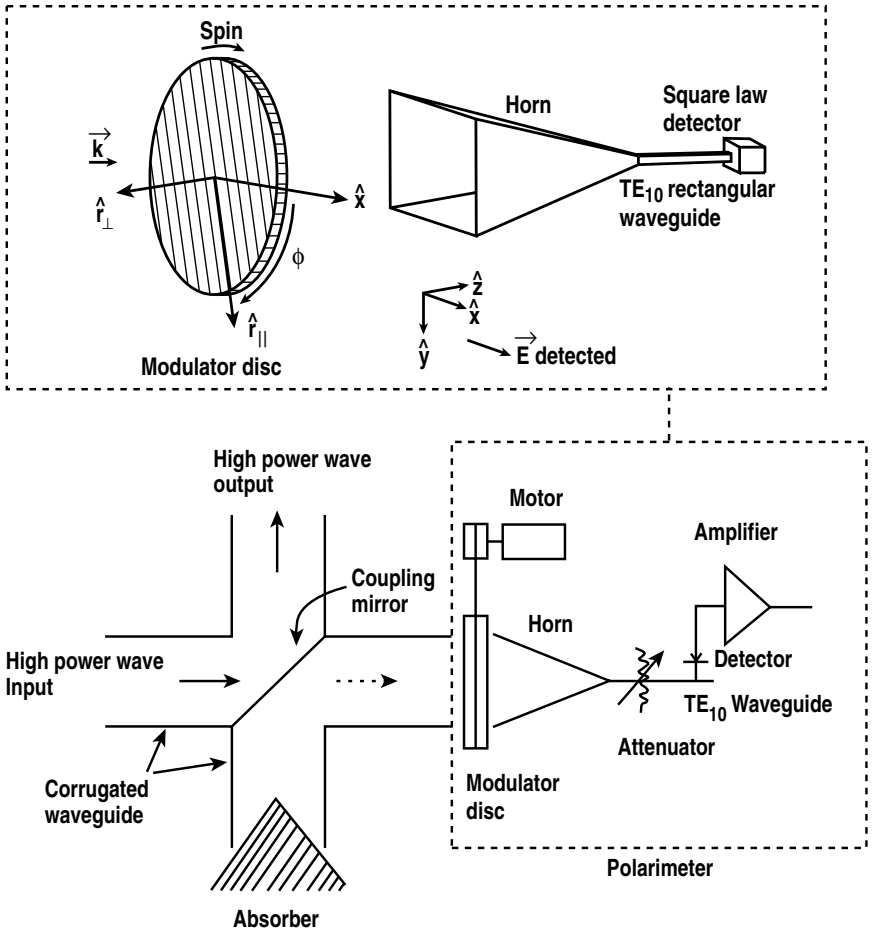

Fig. 6. Schematic diagram of the high power vacuum polarimeter. The rotating birefringent plate modulates the rf detected by a fundamental waveguide system which is then Fourier analyzed to obtain the polarization parameters.

cooling. A cooled version of this mirror is being developed for 1 MW cw operation.

Calibration of the polarimeter at low power allows the rf beam parameters to be calculated directly from the modulated signal detected as the analyzing plate is rotated during a gyrotron pulse. In Fig. 7, a typical example of the measurement at the output of Katya is shown. The polarization is nearly completely linear, but with a tilt angle of about 3°

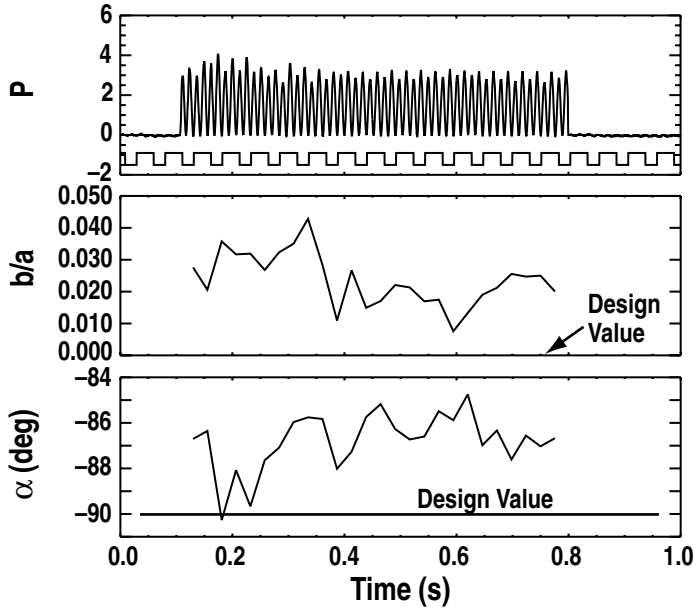

Fig. 7. Raw detected data and post processed data showing the measurements of b/a and α for the output from the Katya gyrotron. A small deviation from horizontal linear polarization of the rf from the gyrotron can result in an admixture of O–mode in the wave excited in the tokamak as indicated by the power deposition profile measurements for oblique injection.

from horizontal. This tilt propagates through the transmission line and polarizer system to appear as an undesired O–mode component in the beam injected into DIII–D, exactly as indicated in the plasma measurements of the power deposition profile.

The polarimeter has been used to characterize all the gyrotron and waveguide systems and the individual characteristics of the separate systems are taken into account in determining the settings for the polarizer mirrors for a particular DIII–D injection geometry. The accuracy of the measurement is ±1° in tilt and 1% in b/a.

Alignment of the rf beam to the waveguide

Alignment of the rf beam and the waveguide for the DIII–D system has always been an issue, since misalignment can result in coupling to lossy modes in the waveguide rather than the desired $HE_{1,1}$ and both

damage to the components and injection of waves with mixed polarizations into the tokamak can occur.

The current alignment procedure is to determine the direction in space of the axis of the rf beam emanating from the gyrotron and to place the optical axis of the two-mirror Matching Optics Unit on this axis. This guarantees that, to high accuracy, the rf beam strikes the center of the first MOU mirror. Micrometer screws on the first mirror are then used to adjust the tilt of this mirror slightly to place the centroid of the beam on the center of the second MOU mirror, which is diagnosed by infrared camera measurements of an rf absorber on the surface of the second mirror. This step is less precise, because the beam is not focused at this point. The final x, y alignment at the waveguide input is determined for short pulses using thermally sensitive paper attached to the waveguide.

This procedure can center the beam to better than 1.0 mm at the waveguide input, which is easy to measure, with coaxiality to better than 0.5 ° which is difficult to measure. This accuracy would yield only a few per cent mode conversion at worst.[12–14] But the measured power losses to the MOU mirrors and structure have always been around 15% for all our systems, which could be due to misalignment. Furthermore, all the alignment is done for short pulses as the gyrotron is turning on, which might be atypical of the situation for longer pulses. Therefore, an independent measurement of the mode mix in the waveguide with long pulse capability was sought.

The device developed for this measurement makes use of the diamond coupling mirror designed for the polarization measurements described above. In the straight through arm of the miter bend, a corrugated waveguide initially carries the coupled low power rf beam. The weaker spurious modes must be separated from the dominant $HE_{1,1}$ mode. After an arbitrary distance, the waveguide wall corrugations end and the wall becomes smooth, causing conversion of the $HE_{1,1}$ mode to $TE_{1,1}$, $TE_{1,2}$, ..., $TM_{1,1}$, $TM_{1,2}$ .... modes, all of which have electric field components at the waveguide center in the $\hat{y}$ direction and no component in the $\hat{x}$ direction. Thus, a fundamental waveguide at the waveguide center oriented to couple to E_y can be used as the $HE_{1,1}$ detector. Spurious modes generated from misalignments either couple to modes which have E_x and E_y components at intermediate radii, say $a/2$, or have nonzero x and y components themselves. For example, the $HE_{2,1}$ mode resulting from either angular or transverse misalignment converts to $TE_{2,1}$, $TE_{2,2}$, ...,$TM_{2,1}$, $TM_{2,2}$, etc. Therefore, the analyzer incorporates two additional fundamental waveguide pickoffs at intermediate radii placed azimuthally at $\theta = 0$ and $\theta = \pi/2$ where $\theta = 0$ is in the horizontal plane and $\theta = \pi/2$ is in the vertical plane. For horizontal polarization incident on

the analyzer, an angular misalignment in the vertical plane excites waveguide modes with $E_x = 0$ at $\theta = 0$, $r/a = 1/2$, but $E_x \neq 0$ at $\theta = \pi/2$, $r/a = 1/2$, and an angular misalignment in the horizontal plane excites modes with $E_x = 0$at $\theta = \pi/2$, but $E_x \neq 0$ at $\theta = 0$. Thus the central detector becomes the monitor for the $HE_{1,1}$ component and the ratio of this signal to the two off-axis signals gives the extent of the misalignment in the x and y planes. A schematic of the analyzer is shown in Fig. 8.

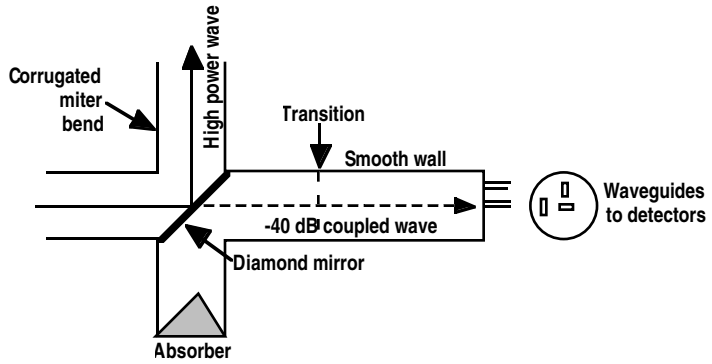

Fig. 8. The alignment analyzer relies on mode conversion from a non-coaxial or non-centered ''$HE_{1,1}$'' beam to modes with off-axis E_x or E_y components. The pickoff mirror couples about –40 dB to the analyzer.

The device is in initial testing stages, so no positive conclusions can yet be drawn, but the preliminary indication is that spurious modes are present at low but detectable levels in the waveguide, that the analyzer behaves as designed and that the alignment procedure outlined above gives excellent axial and transverse alignment.

Parasitic oscillations in the gyrotrons

Two of the three gyrotrons installed at DIII–D exhibit parasitic oscillations.[15,16] Although the low frequency emissions cause difficulties for circuits and nearby equipment, the effect on the gyrotron operation is not pronounced. Although some characteristics of the parasites in the two gyrotrons are the same, in some respects the behaviors are quite different.

The Katya gyrotron has a low frequency parasite at 96 MHz, the radiated intensity of which has been estimated at a few kW. For this gyrotron, the parasite is always present above a threshold electron beam current of about 4 A. At very low currents the exact frequency is not well

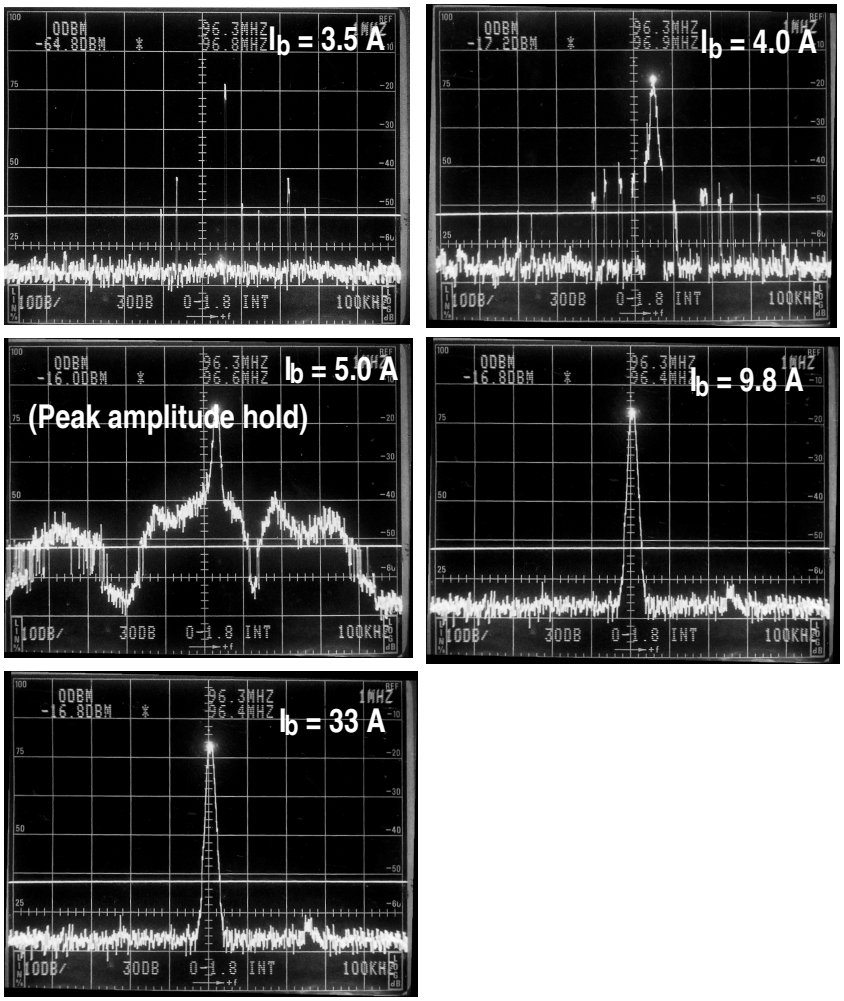

Fig. 9. The parasitic emission spectra on Katya for a range of electron beam currents. Below a threshold current, no parasite is observed. The emission begins sporadically as the beam current is increased and finally locks to a monochromatic output above about $I_b = 12$ A.

determined and sporadic oscillations are observed over a ±5 MHz range centered at 96 MHz. As the beam current is increased, the averaged spectrum fills in with well defined sidebands and harmonics at least to the tenth. At the operating beam current, around 32 A, the spectrum is rather monochromatic. The spectra observed on an antenna near the gyrotron

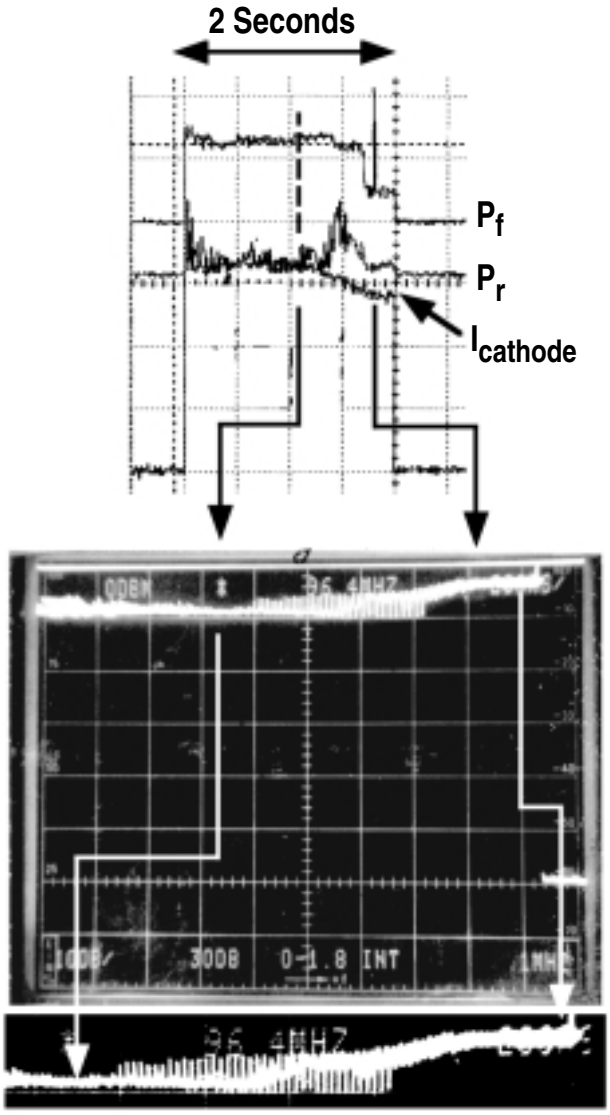

Fig. 10. The amplitude of the Katya parasite increases substantially when the cathode current drops near the end of a long pulse. The increase begins as a series of regularly spaced spikes, the peaks of which eventually define the c.w. parasite amplitude. Decreasing the gun bucking coil current can preserve the constant cathode current, without the increase in parasite amplitude, but the observation may have a bearing on operation for still longer pulses. Sensitivity is 10 dB/cm.

are shown in Fig. 9 with I_b as a parameter. For long pulses greater than about 1.5 sec, there is a clear correlation between an increase in the parasitic emission and a decrease in the electron beam current. In Fig. 10 the spectrum analyzer is tuned to 96 MHz with a 100 kHz bandwidth. When the electron beam current begins to droop, there is a regular series of 10 dB spikes in the parasitic emission, the peaks of which eventually become the new equilibrium emission level. A decrease in the gun bucking coil current decreases the electron pitch angle and restores normal operation at constant current to the end of the pulse, strongly suggesting that reflected electrons trapped in the magnetic mirror between the gun and the cavity are involved.[17] The time constant for the change in beam current at the end of the pulse suggests thermal effects are involved.

Parasitic oscillations in gyrotrons with triode MIGs have rarely been encountered, but are clearly seen on Toto, the gyrotron with diamond window and Gaussian output beam. The observations, however, differ qualitatively from those for Katya. On Toto, the onset of the parasite is characterized by a rapid increase, typically about 10%, in the cathode current. The output spectrum at 110 GHz is practically not affected. In contrast with the spectrum for Katya, the parasitic spectrum for Toto is orders of magnitude less strong, closer to the strengths of broadcast signals. But the spectrum peaks at about the same frequency and similar sidebands are observed. In Fig. 11 the spectra for Toto are shown, while in Fig. 12 the cathode current is shown with the 110 GHz spectrum both before and after the step in current. The spectrum analyzer sensitivity decreases slightly in the presence of the low frequency noise associated with the parasite, but no detectable change in the output power at 110 GHz is observed calorimetrically when the parasite is present.

The Toto parasite is not as ubiquitous as for Katya. In a series of pulses some will exhibit the parasite and some will not. There is a 1:1 correlation between parasitic emission and vacion current, pulses with the parasite having poorer gyrotron vacua, but causality for this has not been identified.

III. Current Drive Results

The ECH system was primarily used during the 1999 experimental campaign in support of experiments requiring high T_e values, such as fast wave current drive studies. The available power from Katya alone was not sufficient for large scale advanced tokamak research and MHD suppression studies that had originally been contemplated. Nevertheless, the sophistication and sensitivity of the analysis of the $j(r)$ profile using the Motional Stark Effect diagnostic has yielded encouraging current

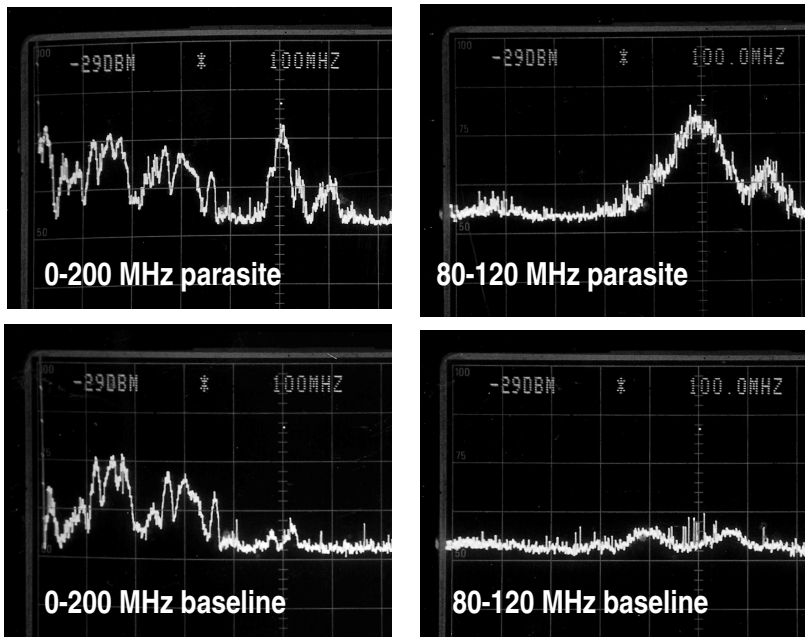

Fig. 11. The low frequency spectra near 100 MHz for Toto during parasitic oscillation. The signals are much weaker than for Katya, but the sidebands are qualitatively the same as the Katya low current spectrum. Sensitivity is 10 dB/cm.

drive results,[18] particularly for off-axis current drive, which will be a critical element of the development of an advanced tokamak concept.

The analysis of non-inductive current drive makes use of the $j(r)$ reconstruction technique of Forest[19] in which magnetic probe data plus the internal magnetic fields measured by Motional Stark Effect spectroscopy give a temporal series of equilibria from which the poloidal flux $\psi(r,t)$ is calculated. The spatial derivative of ψ gives the parallel current density $j_{||}$ as a function of normalized flux and the time derivatives of poloidal flux at fixed poloidal flux give the parallel electric field. In the absence of sawteeth or other strong MHD effects which redistribute the flux, the non-inductive current density $j_{\mathrm{NI}} = j_{||} - \sigma_{\mathrm{neo}} E_{||}$ can then be calculated subject to a neoclassical model for the conductivity. Performing the identical analysis for discharges with and without ECCD allows the non-inductive current density from the bootstrap effect to be separated from the ECCD for both on and off-axis cases.

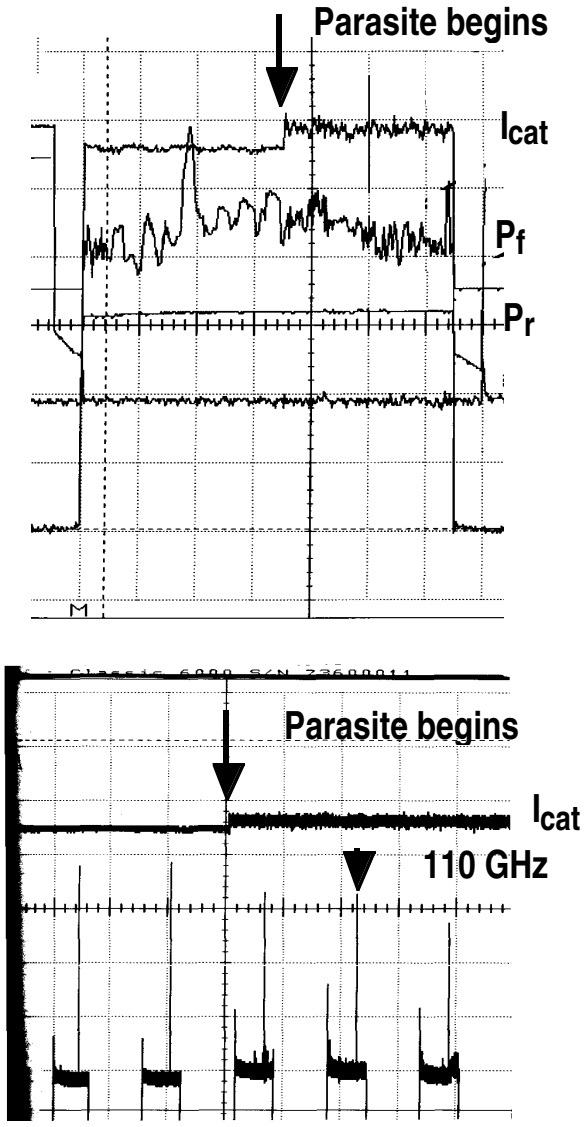

Fig. 12. The region near 110 GHz is shown for a Toto pulse which broke into parasitic oscillation at the point where the cathode current jumps. The 110 GHz output is essentially unaffected, although the additional video noise decreases the sensitivity of the receiver during the parasite.

The injected EC power for the ECCD experiments was about 1 MW. For ECCD near the discharge center, the peak current density driven by electron cyclotron waves was about 90 A/cm^2, corresponding to an integrated driven current of 92 ± 29 kA. This integrated value is in excellent agreement with a quasilinear Fokker-Planck calculation, although the profile of the EC driven current is broader than the calculation predicts. In the case of off-axis ECCD, a peak driven current density of 8 A/cm^2 and an integrated total driven current of 35 ± 13 kA were observed. This value is in agreement with the calculations regarding the peak driven current density, but again, the breadth of the EC driven profile is greater for the experiment than for the Fokker-Planck calculations and the integrated value for currents driven outside the magnetic axis are greater than the calculations predict. Experiments in which ECCD both inside and outside the magnetic axis was measured suggest that the discrepancy between measurement and calculations may be due to the way trapped particle collisionality is handled by the codes, but the initial attempts to model this have not been able to reproduce the better than expected total current drive in the off-axis case.

IV. Future Plans

The DIII–D project has committed to increasing its ECH capability substantially. An additional three 110 GHz gyrotrons in the MW class with long pulse capability, up to 10 sec, are being produced by CPI for phased delivery late in 1999 and early in 2000. These tubes employ diode guns and single disk diamond output windows with Gaussian rf beams. Modulator-regulator power supplies from the MFTF project are being modified to handle two gyrotrons each and a new addition to the DIII–D building is under construction to house the new gyrotrons. Cold test results for the first of the upgrade tubes are shown in Fig. 13 and indicate that the beam is approximately Gaussian down to the –21 dB contour. The first of the upgrade tubes will employ a single mirror external to the gyrotron to focus and direct the rf beam to the waveguide input, a compromise with completely eliminating the matching optics unit with its steering and phase correcting mirrors. The waveguide runs to the new gyrotrons are approximately 85 m, which should introduce approximately 2% additional transmission loss compared with the present installation.

In addition, the DIII–D Project has acquired two Gycom gyrotrons identical to Katya from the Tokamak de Varennes project. Present plans are for these tubes to be installed in time for the 2000 campaign. The flexibility of the ECH launchers is being enhanced in a cooperative project with the Princeton Plasma Physics Laboratory. PPPL is providing a fully articulating launcher assembly for DIII–D which can inject two rf

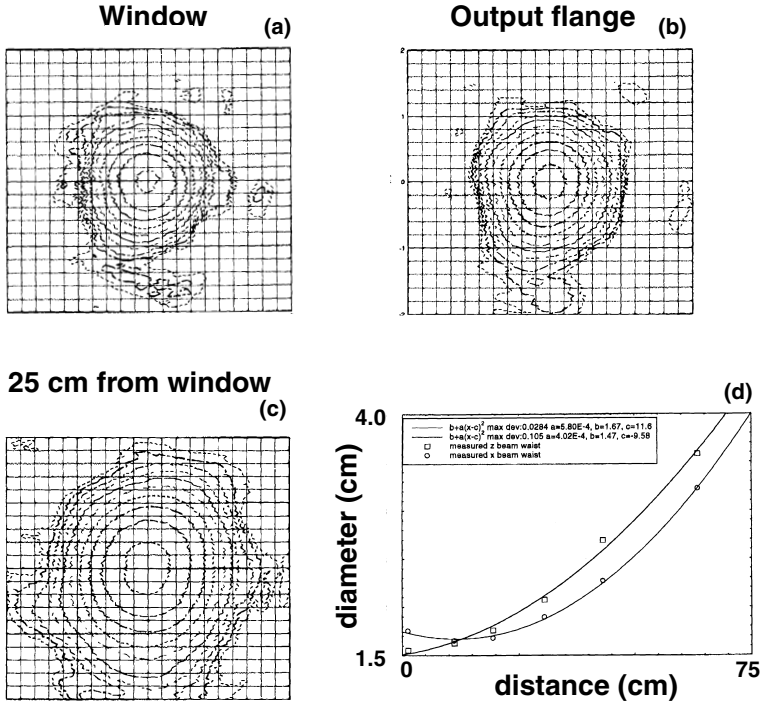

Fig. 13. The three gyrotrons which are being produced by CPI for DIII–D will have diamond output windows and Gaussian rf beams. The cold test results from the first of these gyrotrons are shown in the figure. The output is nearly Gaussian, with a waist at the window. A single mirror system will couple the beam into the waveguide.

beams at variable poloidal and toroidal angles. If the project is successful, launchers for six rf beams will be installed.

V. Conclusions

The 110 GHz gyrotron ECH system on DIII–D has demonstrated many of the key physics results upon which the future advanced tokamak program will depend: Efficient current drive both on and off axis; heating; and required performance parameters. The transmission lines, polarizers, beam steering, dummy loads and diagnostic hardware are working well. Two developmental gyrotrons, which failed in service, have been repaired and are entering a test program. In addition, two

clones of the Gycom gyrotron Katya have been purchased from the Tokamak de Varennes project. An additional group of three production gyrotrons is being produced and tested at CPI. A four-gyrotron system with unit power around 1 MW and pulse lengths of several seconds is planned for the year 2000 experimental campaign with fifth and sixth gyrotrons coming on line during the campaign.

Acknowledgment

This is a report of work supported by U.S. Department of Energy Contract DE-AC03-99ER54463.

References

1. Agapova, M.V., *et al.,* Proc. 20th Int. Conf. Infrared and Millimeter Waves, Orlando (1995) p. 205.
2. Felch, Kevin , *et al.*, IEEE Trans. Plasma Sci. **24**, 558 (1996).
3. Felch, K., *et al.,* Proc. .23rd Int. Conf. Infrared and Millimeter Waves, Colchester (1998) p. 367.
4 Stickel, H., Int J. Electronics **64**, 63 (1988).
5 Katsenelenbaum, B.Z., Semonov, V.V., Rad. Eng. and Elec. Phys. **12**, 223 (1967).
6. Chirkov, A.V., Denisov, G.G., Alexandrov, N.I., Opt. Comm. **115**, 449 (1995).
7. Denison, D.R., Chu, T.S., Shapiro, M.A., Temkin, R.J., IEEE Trans. Plasma Sci. **27**, 512 (1999).
8. Denison, D.R., Kimura, T., Shapiro, M.A., Temkin, R.J., Proc. .22nd Int. Conf. Infrared and Millimeter Waves (Freund, H.P., ed.) Wintergreen (1997) p. 81.
9. Smits, F.M.A., Proc. 8th Joint Workshop ECE and ECRH, Gut Ising (1993) p. 549.
10. Petty, C.C., *et al.*, Proc. 13th Top. Conf. on Applic..RF Power to Plasmas, Annapolis (1999).
11. Ikezi, H., *et al.*, Rev. Sci. Instrum. **70**, 1994 (1999).
12 Ohkubo, K., *et al.*, Proc.T 10th Joint Workshop on Electron Cyclotron Emission and Electron Cyclotron Heating, T. Donne and T. Verhoeven, eds. (World Scientific, 1997) p. 597.
13. Ohkubo, K., et al., Int. J. Infrared and Millimeter Waves **18,** 23–41 (1997).
14. Doane, J.L., Infrared and Millimeter Waves **13,** 123 (1985).
15. Raisky, B.V., Tsimring, S.E., IEEE Trans. Plasma Sci. **24**, n3 (1996).
16 Andronov, A.N., *et al.*, Proc. 20th Int. Conf. Infrared and Millimeter Waves, Orlando (1995) p. 141.
17 Kuftin, A.N., Zapevalov, V.E., Proc. 23rd Int. Conf. Infrared and Millimeter Waves, Colchester (1998) p. 426.
18 Luce, T.C., *et al.*, ''Generation of Lozalized Non-Inductive Current by Electron Cyclotron Waves on the DIII–D Tokamak,'' submitted to Physical Review.Letters.
19 Forest, C.B., *et al.*, Phys. Rev. Lett. **73**, 2244 (1994).